The Current Challenges Review of Deep Learning-Based Nuclei Segmentation of Diffuse Large B-Cell Lymphoma

Gei Ki Tang[1], Chee Chin Lim[2], Faezahtul Arbaeyah Hussain[3], Qi Wei Oung[4], Aidy Irman Yazid[5], Sumayyah Mohammad Azmi[6], Haniza Yazid[7], Yen Fook Chong[8]

Faculty of Electronic Engineering and Technology, Universiti Malaysia Perlis, Arau, Perlis, Malaysia[1, 2, 4, 7]

Sport Engineering Research Centre, Universiti Malaysia Perlis, Arau, Perlis, Malaysia[2, 8]

Hospital Universiti Sains Malaysia, 16150 Kubang Kerian, Kelantan, Malaysia[3, 5, 6]

Department of Pathology, School of Medical Sciences, Universiti Sains Malaysia, 16150 Kubang Kerian, Kelantan Malaysia[3, 5, 6]

Advanced Communication Engineering (ACE) Centre of Excellence, Universiti Malaysia Perlis, Arau, Perlis, Malaysia[4]

***Abstract*— Diffuse Large B-Cell Lymphoma stands as the most prevalent form of non-Hodgkin lymphoma worldwide, constituting approximately 30 percent of cases within this diverse group of blood cancers affecting the lymphatic system. This study addresses the challenges associated with the accurate DLBCL segmentation and classification, including difficulties in identifying and diagnosing DLBCL, manpower shortage, and limitations of manual imaging methods. The study highlights the potential of deep learning to effectively segment and classify DLBCL types. The implementation of such technology has the potential to extract and preprocess image patches, identify, and segment the nuclei in DLBCL images, and classify DLBCL severity based on segmented nuclei counting.**

Keywords—Deep learning; Diffuse Large B-Cell Lymphoma (DLBCL); lymphoma cancer; HoVerNet

I. Introduction

Diffuse Large B-Cell Lymphoma (DLBCL) stands as the most prevalent form of non-Hodgkin lymphoma (NHL), comprising approximately 30% of all cases within this diverse group of blood cancers affecting the lymphatic system. DLBCL is characterized by the rapid proliferation of malignant B-cells in lymph nodes, bone marrow, and other lymphatic tissues. DLBCL can afflict individuals of any age, with a predilection for those over 60 [1]. Given its life-threatening nature and variable clinical outcomes, precise diagnosis assumes paramount importance in the management of DLBCL. The identification and quantification of cell nuclei within tissue samples emerge as crucial for assessing tumor characteristics and grading, thus guiding treatment decisions. Deep learning-based nuclei segmentation offers a promising solution, potentially enhancing diagnostic accuracy and efficiency, to streamline this labor-intensive and time-consuming task.

Accurate diagnosis and staging of DLBCL are critical for determining optimal treatment and prognosis. Nuclei segmentation and classification, a pivotal component of DLBCL tissue image analysis, allow for the identification and quantification of tumor cells. Conventional nuclei segmentation and classification methods are often time-consuming, labor-intensive, and error-prone, making the need for deep learning models readily apparent. However, the complexity of DLBCL samples, such as tissue heterogeneity, staining changes, and complex cell interactions, requires complex and accurate deep learning models to address these challenges [1].

This paper explores the current challenges in nuclei segmentation and classification for DLBCL using deep learning methods. It provides an extensive review of the techniques, preprocessing methods, and segmentation approaches applied to DLBCL analysis. Furthermore, the paper highlights advancements in the field and identifies gaps for future exploration, aiming to inspire further research and innovation in digital pathology.

This paper is structured as follows: Section II reviews related work, highlighting the advancements and gaps in deep learning-based nuclei segmentation and classification for DLBCL. Section III describes the methods, including preprocessing techniques, model architectures, and evaluation metrics. Section IV presents the results and discussions, comparing the performance of state-of-the-art deep learning methods. Finally, Section V concludes the study, summarizing key findings and future research directions. This structure aims to provide readers with a comprehensive understanding of the challenges and contributions in the field.

II. Related Work: Advancements in Diagnosis and Staging of Diffuse Large B-Cell Lymphoma

A. Symptoms, Risk Factors, and Causes of Diffuse Large B-Cell Lymphoma

DLBCL can cause many different symptoms. One of the most common signs is the painless swelling of lymph nodes. These are lumps under the skin, usually found in places like the neck, armpit, or groin. This might happen, along with other signs. For example, losing weight for no reason, always feeling tired, or sweating a lot at night. Also, patients with DLBCL may experience fever from time to time, which further signals the response of the body to lymphoma. Sometimes, DLBCL might affect abdominal organs, leading to symptoms like abdominal pain or swelling. The symptoms show up based on where and how big the bothered lymph nodes or organs are. DLBCL can also have other unique symptoms. These vary based on where

Sponsored by Ministry of Higher Education Malaysia, FRGS grant FRGS/1/2023/ICT02/UNIMAP/02/3 and Universiti Sains Malaysia, RU Top Down grant 1001/PPSP/8070016

in the body they show up. For example, if it is in the chest or lungs, the patient might have trouble breathing, coughing, or having chest pain. Those with DLBCL in their gastrointestinal tract could feel stomach pain, nausea, vomiting, and changes in bowel habits. When DLBCL affects the brain or spinal cord, it might lead to headaches, behavior changes, or even seizures. In some cases, DLBCL could cause problems with the skin. This could look like a rash or bumps. These skin changes might give doctors extra clues during physical examinations.

There are several risk factors and causes that have been identified. Advancing age is a prominent factor, as DLBCL is more prevalent in individuals over the age of 60, and the incidence increases with age. This age-related susceptibility suggests a cumulative effect over time, possibly linked to cellular changes and immune system alterations associated with ageing. A compromised immune system, whether due to medical conditions such as Human Immunodeficiency Virus/Acquired Immunodeficiency Syndrome (HIV/AIDS) or the use of immunosuppressive drugs post-organ transplant, is another significant risk factor [2]. The impaired immune surveillance in these scenarios may create an environment conducive to the uncontrolled growth of lymphoid cells, fostering the development of DLBCL.

The Epstein-Barr virus (EBV), belonging to the herpesvirus family, has been linked to an increased risk of DLBCL, particularly in immunocompromised individuals [3]. The ability of EBV to infect B-cells and potentially contribute to the transformation of these cells underscores its role in the lymphoma genic process. Besides, genetic factors also contribute, with a family history of lymphomas potentially elevating the risk. While the specific genetic mechanisms are not fully elucidated, ongoing research aims to uncover the intricate interplay of genetic and environmental factors in DLBCL development [2]. Other factors, such as autoimmune diseases and certain chemical exposures, have been explored for their potential roles in lymphomagenesis, though their associations remain complex and multifaceted.

B. Diagnosis Method and Staging of Diffuse Large B-Cell Lymphoma

DLBCL is typically diagnosed by removing a swollen lymph node or taking a sample of tissue from it and examining it under a microscope. This involves a minor procedure known as a biopsy, which is usually performed under local anesthesia or through a minor operation. Following the biopsy, expert pathologists use special staining, a test called flow cytometry, and chromosome analysis to determine the exact variant of DLBCL. DLBCL is also diagnosed using blood tests and imaging tests. Blood tests can help determine the overall health of the patient and detect any abnormalities in the blood cells. To determine the location and extent of the disease, imaging tests such as Magnetic Resonance Imaging (MRI) scans, Computed Tomography (CT) scans, Positron Emission Tomography (PET) scans, and ultrasounds are used. Apart from that, the current standard diagnosis method for DLBCL includes two tests: Fluorescence In-Situ Hybridization (FISH) tests and Immunohistochemistry (IHC) tests [4].

The staging of DLBCL depends on the extent of the disease and the organs involved. The Ann Arbour staging system is commonly used to stage DLBCL for lymphoma. It classifies the disease into four stages of involvement, namely Stages I, II, III, and IV [5]. Stage I has been described because the cancer is found in the lymphatic zone or in only one organ. Stage II is indicated because cancer is found in two or more lymph nodes on one side of the lung or in one limb and in one or more lymph nodes on the same side of the lung. Furthermore, cancer found in different parts of the lymph nodes or on either side of the diaphragm is stage III. Lastly, stage IV means that the cancer has spread to one or more organs outside the lymphatic system, such as the liver, lungs, or bones.

1) Biopsy of Diffuse Large B-Cell Lymphoma: A biopsy is a crucial diagnostic method for DLBCL, which allows for the presence or absence of certain genetic alterations. In this procedure, a sample of the affected lymph node or tissue is extracted and examined under a microscope [6]. Immunohistochemical staining and molecular tests are then employed to detect the expression of MYC gene rearrangements. The presence of MYC rearrangements classifies the lymphoma as MYC+, indicating a potentially more aggressive form. Conversely, if there is no evidence of MYC rearrangements, the lymphoma is classified as MYC-.

2) Blood tests: Blood tests are essential in diagnosing DLBCL. A complete blood count (CBC) assesses various blood components, including white blood cells. Elevated white blood cell counts may indicate the presence of lymphoma. Being that B-cells grow and become mature in the bone marrow, the CBC count tests for anemia, thrombocytopenia, and/or leukopenia indicate the extent of bone marrow involvement in DLBCL.

Furthermore, the LDH level is a helpful predictor of treatment response, recurrence, and the severity of DLBCL. Increased levels of potassium, phosphorus, and uric acid combined with a drop in calcium could be signs of tumor lysis syndrome, a condition that can develop during chemotherapy. LDH levels, a specific blood marker, can be indicative of lymphoma activity. Elevated LDH levels may suggest a more aggressive disease. While these blood tests do not directly determine MYC status, abnormal results can prompt further investigations, including imaging studies and biopsies.

3) Imaging tests: Imaging tests are essential components of the diagnostic process for DLBCL, providing valuable information about the extent of the disease and its characteristics. MRI uses strong magnetic fields and radioactive waves to generate detailed images of the internal structures of the body. In DLBCL diagnosis, MRI is useful for assessing the involvement of lymph nodes and surrounding tissues, aiding in the accurate staging of the disease [7]. It offers high-resolution images that aid in determining the size, location, and characteristics of lymphoma masses. Besides, CT scans employ X-rays from multiple angles to create detailed, cross-sectional images of the body [7], [8]. CT scans are valuable in identifying and measuring lymph nodes affected by DLBCL. They help in assessing the extent of the disease, determining the stage, and identifying whether the lymphoma has spread to other organs or tissues.

Other than that, ultrasound is also one of the imaging techniques used to diagnose DLBCL. Ultrasound employs high-frequency sound waves to create real-time images of internal organs and tissues. While less commonly used than other imaging modalities, ultrasound can assist in evaluating abnormalities in lymph nodes. It is particularly useful for examining superficial lymph nodes and assessing potential changes in organ structures caused by lymphoma. Other than that, a PET scan is suitable to detect the progression of tumors and cancer. A PET uses a radiotracer to show the differences between healthy tissues and cancerous tissues. A radiotracer is injected into the patient, and the cancerous cells absorb more of the radiotracer. PET will detect the radiation given off by the tracer and produce color-coded images of the body that show both healthy and cancerous tissues. A special camera from a PET scan detects the radiation emitted by these cells. PET scans highlight areas with increased metabolic activity, helping to identify active lymphoma sites [7]. This is crucial for determining the extent of DLBCL, assessing response to treatment, and locating residual or recurrent lymphoma. In short, these imaging methods provide valuable information about the size, location, and characteristics of lymphoma lesions, aiding in the accurate diagnosis, staging, and ongoing management of DLBCL.

C. Current Standard Diagnosis Method

The current standard diagnosis method for DLBCL involves Fluorescence In-Situ Hybridization (FISH) tests and Immunohistochemistry (IHC) tests. The FISH test is a technique that is essential for identifying genetic abnormalities such as MYC translocations in DLBCL and offering insights into the severity of the disease. Besides, the IHC test is a method that involves the expression of specific proteins and helps in characterizing DLBCL subtypes, such as GCB subtypes and ABC subtypes. By integrating the FISH and IHC, it provides a holistic evaluation, combining genetic and protein expression data to guide accurate diagnosis, subtype classification, and personalized treatment planning for individuals with DLBCL.

1) Fluorescence In-Situ Hybridization (FISH) Test: Fluorescence In-Situ Hybridization (FISH) method is a molecular technique used to detect and locate the presence or absence of specific DNA sequences on chromosomes [4]. It uses fluorescent light that binds to only those parts of the chromosome that show a high degree of sequence complementarity. The FISH method is used to identify specific genetic abnormalities, such as the rearrangements of the MYC, BCL2, and BCL6 genes, to diagnose DLBCL [4]. The purpose of FISH in diagnosing DLBCL is to provide a more accurate diagnosis, which can guide treatment decisions. It enables the precise detection of genetic abnormalities that could be driving diseases like DLBCL [22]. One of the studies that used FISH methods for DLBCL analysis was conducted by Blanc Durand et al. [14]. The authors worked with pre-therapy FDG-PET/CT scans from 733 DLBCL patients.

FISH analysis, which can be performed using dual-color and dual-fusion cleavage probe methods, is a highly sensitive and accurate technique for detecting oncogene amplification in human tissue samples. However, due to the high variability in MYC breakpoints, it may not identify all MYC abnormalities. Furthermore, the FISH method has some limitations and shortcomings. This method may not be universally applicable to all diseases due to its labor-intensive and demanding nature, making it a time-consuming procedure. The need for expensive techniques, especially when using fluorescence microscopy, is specific and sensitive, emphasizing the importance of elucidating the genetic status of DLBCL.

2) Immunohistochemistry (IHC) Test: Immunohistochemistry (IHC) is a method used to visually detect the presence of specific proteins in cells or tissues. It involves the use of antibodies that bind to these proteins and a detection system that uses a colored or fluorescent dye to visualize the binding [23]. IHC studies have evolved, emerging as the most widely used test to characterize cancers and identify hidden metastatic sites, particularly in lymph nodes. The method is based on the specific binding of antibodies to antigens, allowing the detection and specific localization of molecules in cells and tissues. The primary analysis is typically conducted using a light microscope [9]. IHC plays a crucial role in cancer diagnosis, especially when specific tumor antigens are overexpressed in certain malignancies. Notably, IHC offers significant advantages, particularly in settings with limited resources and drawbacks. IHC provides qualitative information about the presence or absence of specific antigens but does not quantify the expression levels.

In DLBCL, IHC is used to identify abnormal protein expression of certain genes. For instance, IHC can be used as a screening test to identify cases of DLBCL and identify overexpression of the BCL2 protein, which is associated with a poor prognosis in DLBCL [23]. The purpose of IHC in diagnosing DLBCL is to provide a more accurate diagnosis, which can guide treatment decisions. It is an inexpensive and rapid test that can identify abnormal protein expression in mutated genes [23]. Furthermore, the intensity of marker expression can have prognostic implications. This limitation may impact the precision of the diagnosis. Apart from that, DLBCL comprises different subtypes with varying clinical behaviors. IHC alone may not always reliably distinguish between GBC subtypes and ABC subtypes. Gene expression profiling or additional molecular tests might be required for a more accurate subtype classification [10]. Also, IHC primarily provides information on protein expression but may not directly reveal underlying genetic alterations, such as gene mutations or chromosomal abnormalities.

III. Related Work: Image Processing Methods and Artificial Intelligence Algorithms

A. Image Processing Methods

1) Image patches: Image patches are small, square regions of an image used for feature extraction. It plays a crucial role in identifying the regions of interest (ROIs) in medical images of DLBCL patients. These patches are needed for image processing tasks and algorithms such as image analysis, feature extraction, and applications involving AI algorithms. Besides,

it is normally used at the local level to analyze and manipulate image data and enable us to concentrate on specific areas of interest, such as structures and textures. This approach yields more detailed and accurate results, allowing feature extraction and providing reliable decisions. The size and shape of patches can vary depending on the task and requirements. It can range from a single pixel to a predefined window that features multiple pixels. The segmentation techniques may organize identical areas and distinguish them from the background by analyzing the color, appearance, or pixel's intensity, which allows for tasks like object detection and recognition.

Patch size and resolution are determined by specific applications and dataset requirements. For example, El Hussien et al. [16] obtained an overall mean Dice score of 0.825 from a quantitative assessment that included 15 manually annotated patches of 256×256 pixels. Furthermore, they conducted a study in which 10 Chronic Lymphocytic Leukemia (CLL), 12 accelerated Chronic Lymphocytic Leukemia (aCLL), and 8 Richter's Transformation (RT) digitally stained hematoxylin and eosin (H&E) slides from a lymph node excisional biopsy were chosen at random. The study used Aperio AT2 scanners to scan the slides, with an optical resolution of 20× magnification. These slides came from various patients, and a total of 25, 28, and 21 ROIs were from CLL, aCLL, and RT, respectively.

Wójcik et al. [17] employed 37,665 H&E-stained images obtained at 40× magnifications from a solitary WSI of DLBCL lymph nodes. Each image tile, sized at 512×512, underwent segmentation, with bounding boxes outlining individual nuclei, although no cell labels were provided. The images are standardized to 448×448 pixels, with additional randomly cropped tiles to augment the training dataset. Li et al. [18] focused on DLBCL tissue sections, capturing pathologic images initially at 400× original magnifications. The study began with 500 images obtained from labelled H&E-stained sections of lymph nodes. Apart from that, Swiderska-Chadaj et al. [20] digitized 42 H&E slides of DLBCL using a Pannoramic 250 Flash II scanner at an objective magnification of 20×. These slides, with a pixel size of 0.24 µm, comprised an external validation set, allowing assessment across different hospital protocols.

Bándi, P. et al. [21] collected 100 WSI from various medical centers, comprising 10 tissue samples across different staining categories. Image patches were extracted from annotated areas using mask images according to the different pixel spacings, being 62.5, 250, and 10000 µm at respective resolutions of 0.5, 2, and 8 µm. Other than that, the research by Shankar, V. et al. [27] involves the H&E-stained tissue cores, pinpointed by hemapathologists using Qupath, for extracting image patches. These patches were obtained at 40× magnifications from each core. Based on the study by Swiderska-Chadaj, Z. et al. [29], the training dataset was derived from H&E-stained specimens. The image patches, each sized at 512×512 pixels, were extracted from slides at 5× magnification level with a pixel size of 1 µm for optimal analysis. Perry, C. et al. [31] involved a self-supervised phase, which included the slides to be scanned at either 20× or 40× magnifications. The 40× images were converted to 20× for analysis. The WSI was divided into smaller patches used as model input by using patches of size 384×384 pixels.

Studies by El Hussien et al. [16], Wójcik et al. [17], and others have demonstrated the utility of image patches in DLBCL analysis, achieving high mean Dice scores and effectively capturing relevant features. However, while image patches excel in local analysis, they may struggle with capturing global context, which is crucial for a comprehensive understanding and diagnosis of DLBCL. Besides, weaknesses such as the absence of cell labels in datasets and variability in staining and scanning methods across the study by Wójcik et al. [17] pose challenges to consistency and accuracy. Opportunities lie in the potential for standardizing imaging and analysis protocols, augmenting training datasets with synthetic images, and applying transfer learning to enhance model performance. Conversely, threats include inter-laboratory variations that may limit model generalizability, computational resource constraints, and data privacy concerns related to patient-derived images. These factors collectively underscore the complexities and prospects of advancing the field of digital pathology for hematological malignancies.

2) Preprocessing methods: Preprocessing is a technique that is required to prepare image data for model input. For example, the fully connected layer of a CNN required that all images be stored in arrays of identical size. Model preprocessing may also reduce the training period and accelerate model inference. If the input images are very large, diminishing the size of the images will drastically reduce the time required to train the model without affecting model performance significantly. Basically, the preprocessing steps include orientation, resize, random flips, grayscale, and other different exposures that inhibit unforeseen distortions or improve certain characteristics of images essential to the deep learning pre-trained model.

Hamdi, M. et al. [11] used Gaussian filter to smooth the images, a Laplacian filter for edge detection, color normalization for standardization, resizing to a consistent resolution, and the use of Gradient Vector Flow for additional feature extraction. Besides, Vrabac et al. [12] focused on the employment of various preprocessing techniques to prepare histopathological images for analysis. The authors arranged the images in tissue microarrays (TMAs) and performed cell nucleus extraction from H&E-stained images. Additionally, they extracted features such as maximum area, minimum area, hull area, perimeter nucleus, maximum angle, ellipse perimeter, and ellipse area to capture morphological characteristics [12]. Basu and his team developed novel preprocessing methods for DLBCL classification. Although the exact preprocessing steps were not specified, the authors introduced in their attention map feature transformer, feature fusion techniques, and a specific loss function to improve the performance of the DLBCL classification model [13].

In the study conducted by Blanc-Durand et al. [14], they underwent a series of preprocessing steps. These steps included resampling, padding, cropping, and scaling of PET and CT

image data to ensure consistency. Additionally, adaptive thresholding was applied to segment images, and various features related to tumor characteristics, such as tumor heterogeneity, textural features, total tumor surfaces, and spatial dispersion, were extracted to provide a comprehensive set of features for classification. Ferrández and colleagues employed preprocessing methods tailored to medical imaging [15]. Gaussian filtering was applied to enhance image quality, and metabolic tumor volume (MTV) and standard uptake value (SUV) were computed to quantify metabolic activity. The authors also considered features related to tumor dissemination and textural features to capture the heterogeneity of DLBCL tumors.

El Hussien, S. et al. [16] focused on the preprocessing methods that involved annotating ROIs, calculating the ratio of the segmented nuclear contour area to its convex area, and measuring hull areas within these annotated regions. Besides, Graham, S. et al. [19] involved preprocessing methods such as Otsu thresholding, pixel intensity manipulation, color adjustments, and extraction of textural features to capture various characteristics within the images. Furthermore, Ferrández, M. C. et al. [24] studied how their preprocessing workflow incorporated normalization techniques, filtering procedures, max-pooling layer utilization, and rectified linear unit (ReLU) operations, possibly aimed at enhancing image quality and extracting relevant features. Other than that, Mohlman, J. S. et al. [25] involved the preprocessing methods, which are normalization techniques and edge detection methods, and utilized a deep network-based pixel-level concept, indicating a complex approach to feature extraction.

The other studies, including Farinha, F. et al. [26], Shankar, V. et al. [27], Jiang, C. et al. [28], Swiderska-Chadaj, Z. et al. [29], Steinbuss, G. et al. [30], Perry, C. et al. [31], Lisson, C. S. et al. [32], have been using the same preprocessing techniques. Their methodologies involved various preprocessing techniques, such as normalization, quality control thresholds, machine learning algorithms, filtering, and feature selection, aiming to enhance image quality, extract informative features, and facilitate accurate DLBCL classification.

Hamdi et al. [11], Vrabac et al. [12], and others have employed various preprocessing techniques tailored to DLBCL analysis, aiming to enhance image quality and extract informative features. While preprocessing can improve model performance and accelerate training, aggressive preprocessing may distort image features, leading to erroneous analysis results. The various preprocessing techniques used in DLBCL image analysis, such as feature extraction and Gaussian smoothing, highlight a reliable strategy for improving diagnostic accuracy. Despite their differences, these methods work together to provide a classification process that is more precise and effective, demonstrating the dynamic interaction between pathology-specific technology and medical knowledge.

3) Data augmentation: Data augmentation is a method for improving performance. It entails changing the color, brightness, or contrast of the existing training data by cropping, flipping, rotating, scaling, or changing the color, brightness, or contrast. Data augmentation can increase the variety and scope of the training data. This can minimize excessive overfitting and make the model more resilient to different inputs. To implement data augmentation techniques for CNN training data, Python libraries such as TensorFlow, Keras, and OpenCV are used.

Basu, S. et al. [13] augmented their datasets through diverse techniques such as image rotations, horizontal and vertical flips, zoom scaling, as well as horizontal and vertical shifts. Wójcik, P. et al. [17] incorporated cell patch embedding, patch aggregation, random resizing, cropping, color jittering, and random flipping, aimed at organizing and augmenting image data for analysis. Other than that, Graham, S. et al. [19] used data augmentation methods such as flipping, rotation Gaussian blur, and median blur for enhanced feature variability. Bándi, P. et al. [21] also applied diverse augmentation techniques like horizontal mirroring, rotation, scaling, color, and contrast adjustments, additive Gaussian noise, and Gaussian blur for image enhancement and feature variability.

Mohlman, J. S. et al. [25] augmented their datasets through random horizontal flipping of images and random alteration of contrast, while Swiderska-Chadaj, Z. et al. [29] includes data augmentations such as brightness, contrast, saturation, rotation, gaussian noise, and gaussian blur. Besides, the data augmentation for the study of Perry, C. et al. [31] includes color jittering and channel shuffle. The study of Lisson, C. S. et al. [32] includes data augmentations such as random flip, gaussian blur, and gaussian noise.

Basu et al. [13], Wójcik et al. [17], and others have utilized data augmentation techniques to enhance the variability of DLBCL image data and improve model performance. However, the effectiveness of data augmentation depends on the appropriateness of the augmentation strategies and the quality of the generated samples. Moreover, excessive augmentation may introduce synthetic artifacts or distortions that do not accurately represent real-world variability. By simulating a variety of variations in medical images, these techniques improve generalization to new data and increase the size of the training dataset. However, the creation of high-quality samples and the choice of suitable tactics are prerequisites for the success of data augmentation. Excessive or improper augmentation can result in synthetic artefacts or distortions that may not accurately represent clinical scenarios and lead to inaccurate predictions, despite being necessary for the robustness of the model. As a result, the ability of data augmentation to provide realistic and clinically relevant variations without compromising the diagnostic integrity of the images serves as a gauge for its efficacy.

B. Artificial Intelligence Algorithm

The process of transferring information, data, and cognitive abilities to machines is known as AI. The primary objective of AI is to create independent machines with human-like thought and behavior. Through learning and problem-solving, these machines can mimic human behavior and carry out tasks. For resolving complex issues, most AI systems mimic natural intelligence. A branch of AI called machine learning employs statistical techniques to let machines learn from experience. Deep learning is a branch of machine learning that processes

information for specific analysis and subsequent action by modelling parts of the human brain with multi-layer neural networks. Hence, AI can be expressed more simply as the overall system, with machine learning and deep learning being its subsets. Deep learning is a subset machine learning, which employs neural networks to learn from massive amounts of data. The relationship between AI, machine learning, and deep learning are shown in Fig. 1.

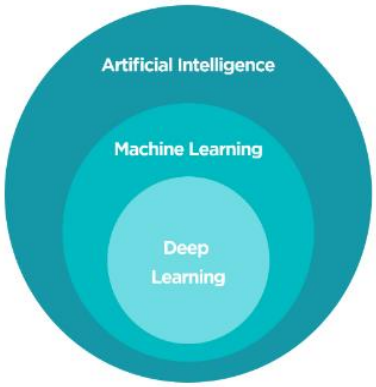

Fig. 1. Hierarchical relationship between artificial intelligence, machine learning, and deep learning.

C. Machine Learning Approaches

Machine learning can be used to extract features from medical images and classify them as either healthy or cancerous. These algorithms can be trained on large datasets of medical images to learn how to identify those that are indicative of cancer. Once trained, these algorithms can be used to analyze and classify new medical images.

1) Multilayer Perceptron (MLP): An artificial neural network type called a Multilayer Perceptron (MLP) is frequently used for machine learning tasks like regression and classification. MLP can be used in the image processing and classification of DLBCL to identify features in medical images and categorize them as either benign or malignant. MLP is a multi-layered input layer, one or more hidden layers, and an output layer, which make up the feedforward neural network [40] [41], [42]. Every single node in the network's hierarchy is connected to it, and every connection has a weight. During training, the weights are changed to minimize the discrepancy between the expected and actual outputs. The structure of MLP in machine learning is shown in Fig. 2.

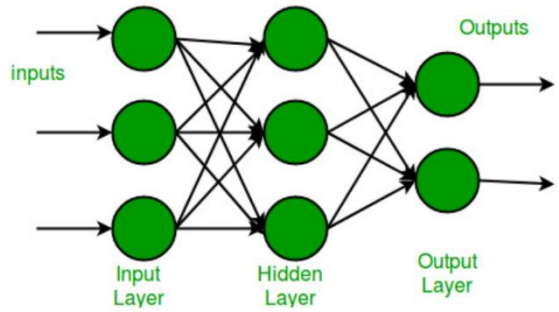

Fig. 2. Structure of Multilayer Perceptron (MLP) in Machine Learning [40].

The MLP emerges as a pivotal tool across several studies in medical imaging and data analysis. Carreras et al. [33], [34], [37] extensively employed MLP, alongside other statistical methods, in various scales and contexts. In their investigations involving 414 and 100 cases, respectively, they utilized MLP along with Mann-Whitney U tests, Kaplan-Meler analysis, and multivariate Cox regression to discern hazard ratios and risks. Additionally, Wagner et al. [35] and Chen et al. [36] explored different facets of image processing; while Wagner utilized grayscale images and specific filtering techniques like Rudin-Osher-Fatemi (ROF), Chen focused on feature extraction from biopsy specimens using solidity features and ROI annotation. Bhattamisra et al. [38] and Achi et al. [39] emphasized the role of MLP in handling vast geometric data and image analysis, respectively.

2) Radial Basis Function (RBF): In machine learning, the Radial Basis Function (RBF) is a kernel function that is used to identify a regression line or non-linear classifier. RBF is capable of being used to extract characteristics from clinical pictures and categorize them as either benign or malignant in DLBCL image manipulation and classification. RBF compares two inputs according to how far apart they are in a high-dimensional space. The Gaussian kernel, also referred to as the RBF kernel, can be found in the Eq. (1).

$$K(x, x') = e^{-\gamma||x-x'||^2} \quad (1)$$

where,

$$K(x, x') = \textit{Radial basis function}$$

$$\gamma = \textit{Width of the kernel}$$

The RBF stands out as a key computational approach utilised in several studies, notably alongside the MLP in medical data analysis. Carreras et al. [33], [34], [37] incorporated RBF networks in conjunction with MLPs to process and interpret diverse datasets. Specifically, they employed RBF alongside MLP in their analyses involving various statistical tests such as Mann-Whitney U tests, Kaplan-Meler analysis, and multivariate Cox regression, elucidating hazard ratios and risks across different case volumes. The utilisation of RBF underscored its relevance in enhancing the MLP's performance and classification and prediction taste, contributing to the robustness of models used in medical imaging and genomic analysis. The application of RBF within MLP architectures demonstrated its capacity to handle complex data structures, aiding in the extraction of valuable insights from medical datasets.

D. Deep Learning Approaches

In recent decades, there has been a lot of interest in the advanced field of ML known as DL. It has been extensively employed in numerous applications and has proven to be a successful ML technique for a few challenging problems. DL algorithms, such as CNN, are particularly effective for image processing and classification tasks. CNNs can learn to identify complex patterns in medical images and classify them with high accuracy. For example, CNN can be trained to identify specific features in medical images of DLBCL patients, such as the size and shape of a cancerous cell and use this information to

classify the images as either healthy or cancerous. Identification and manual classification are challenging tasks, particularly in the medical field. Thus, using different architectures to improve the classification of images requires the application of DL. The goal of image classification is to effectively identify and categorise the biomedical characteristics that have important benefits for many research and development domains.

Among deep learning architectures, such as U-Net, ResNet, and HoverNet have emerged as popular choices for nuclei segmentation in medical imaging. Recent studies have compared the performance of these architectures in the context of DLBCL segmentation and classification [11]-[39]. For example, U-Net demonstrated moderate success in segmenting nuclei but required extensive preprocessing and data augmentation to achieve consistent results. ResNet-based models showed improved feature extraction capabilities but were prone to overfitting with smaller datasets. HoVerNet excelled in cases involving nuclear overlap and heterogeneity but at the cost of increased computational complexity. These findings highlight the need for continued exploration and optimisation of deep learning methods tailored specifically to the nuances of DLBCL.

E. Convolutional Neural Network (CNN) Architecture

CNN are a subset of neural networks that are particularly adept at processing data using network-like topologies such as images. The binary representation that represents visual data is what makes up a digital image. It is made up of a grid-like arrangement of pixels with pixel values to indicate the colour and brightness of each pixel.

In the CNN architecture, it typically has three layers. First, there is the convolution layer. The convolutional layer is the fundamental component of a CNN, carrying the majority of the network's computational load. It works by performing a dot product operation between a limited area of the input image called the receptive field and a learnable matrix called a kernel. The kernel functions across the height and width of the picture during the forward pass. It is less extensive systematically but greater in depth than the image. This motion creates a 2D activation map that illustrates the response of the kernel at every spatial location. The total area of this activation map is determined by the sliding motion of the kernel, also known as the stride. The formula for the convolutional layer is expressed as in Eq. (2):

$$W_{out} = \frac{W-F+2P}{S} + 1 \quad (2)$$

where,

$W_{out} = Output\ volume\ size$

$W = Squared\ input\ image$

$F = Receptive\ field\ size$

$P = Amount\ of\ zero\ padding$

$S = Stride$

Second is the pooling layer. By calculating a summary statistic from the outputs in the vicinity, the pooling layer substitutes the network's output at specific points. This aids in shrinking the representation's spatial size, which lowers the quantity of calculations and weights needed. Each of the sections of the representation is processed independently for the pooling operation. The formula for the pooling layer is expressed in Eq. (3):

$$W_{out} = \frac{W-F}{S} + 1 \quad (3)$$

where:

$W_{out} = Output\ volume\ size$

$W = Squared\ input\ image$

$F = Receptive\ field\ size$

$S = Stride$

Nonetheless, the most widely used method is max pooling, which provides the neighbourhood's maximum output. Lastly, the third layer involved is a fully connected layer (FC layer). As in a regular fully convolutional neural network (FCNN), all neurons in this layer are fully connected to all neurons in the layer that comes before and after. Hence, it can be calculated using the standard method of matrix multiplication and the bias effect. The relationship between the input data and the output is mapped with the aid of the FC layer.

Based on DLBCL nuclei segmentation in CNN, it normally uses a pre-trained model, epoch, optimiser, learning rate, and decay rate. A single run through the complete training dataset is referred to as an epoch. The model is trained on a new batch of dataset samples during each epoch. One hyperparameter that indicates the number of times the model is trained on the complete dataset is the number of epochs. Besides, during training, an optimiser is an algorithm that modifies the neural network's weights. The optimiser determines the way to modify the weights to minimise the loss by utilising the weights' gradients and the loss function. Also, learning rate refers to the weights of the neural network, which are updated to a certain extent based on the hyperparameter. A low learning rate can lead to more stable training, as a high learning rate will trigger the algorithm to converge more rapidly, potentially leading to unstable learning. Apart from that, decay rate controls the amount of learning rate that decreases following each epoch. The learning rate may decrease too rapidly or too slowly, depending on the decay rate, while a high decay rate may decrease the learning rate in a rapid way. Also, a pre-trained model in CNN is a model that is ready to use as the basis for a new model since it has been trained on a sizable dataset. When a new model needs a good setting, pre-trained models can help it perform better. Based on the studies [11-32], there are a few pre-trained models that are being utilised, such as DenseNet-201 [13], ResNet-50 [12], HoVerNet [12], [16], [17], [19], and U-Net [14], [15], [20], [24], [26], [28], [29]. The summaries for methods on DLBCL by using CNN architectures and ML are tabulated in Table I and Table II (Appendix).

1) HoVerNet: DLBCL nuclei segmentation is the process of highlighting nuclei in pathology images. HoVerNet, a specialised network, excels at this task by incorporating multiple branches for segmentation and classification into a unified framework. It takes advantage of nuclear pixel distances

from their centres of mass, which is critical for segmenting clustered nuclei found in DLBCL images. The network's dedicated up sampling branch aids in the classification of different nuclear types. The efficacy of HoVerNet in DLBCL nuclei segmentation stems from its ability to handle complex arrangements, which contributes to improved pathology image analysis.

Based on the study by Vrabac et al. [12], they employed HoVerNet as their chosen pre-trained model. Besides, Hussein et. al. [16] utilised HoVerNet as their pre-trained model for the analysis of CLL, aCLL, and RT cases. Wójcik et al. [17] employed HoVerNet as their chosen pre-trained model, training it for 800 epochs. Lastly, Graham et al. [19] use HoVerNet as their pre-trained model, training it for 50 epochs with the Adam optimiser.

2) U-Net: U-Net, a well-known CNN architecture, is widely used in image segmentation, including the segmentation of DLBCL nuclei. U-Net extracts image features from the encoder and reconstructs a segmentation map from the decoder, which is made up of an encoder and decoder network linked by a bottleneck layer. U-Net can be differentiated into two-dimensional U-Net (2D U-Net) and three-dimensional U-Net (3D U-Net).

Based on the study by Blanc-Durand et al. [14], they utilised the 3D U-Net architecture as the pre-trained model for their pre-therapy FDG-PET/CT scans from 733 patients with DLBCL. The optimizer used was Adam. Similarly, Ferrández et al. [15] employed the 3D U-Net architecture as the pre-trained model. The optimisation was conducted using the Adam optimiser, with an epoch setting of 200. The learning rate was set at 0.00005, alongside a decay rate of 0.000001. Furthermore, Swiderska-Chadaj et al. [20] utilised U-Net as their chosen pre-trained model. In addition, Ferrández et al. [24] employed 3D U-Net as their chosen pre-trained model. The optimiser used was Adam, with an epoch setting of 200, a learning rate of 0.00005, and a decay rate of 0.000001. Other than that, Farinha, F. et al. [26] employed U-Net as their chosen pre-trained model. The epoch setting of 150, a learning rate of 0.0001. Lastly, Jiang, C. et al. [28] utilised 3D U-Net model and was trained for 1000 epochs with a learning rate of 0.01 and Nesterov momentum set to 0.99. According to the work by Swiderska-Chadaj, Z. et al. [29], the U-Net model was pre-trained using the Adam optimizer for 500 epochs with a learning rate of 0.0005.

3) ResNet-50: ResNet-50, which is made up of many residual blocks, aids in the learning of complex characteristics that are required for accurate nuclei segmentation and classification and performs well in DLBCL nuclei segmentation. The depth of its architecture allows for the capture of complicated nuclear characteristics, improving segmentation precision in DLBCL pathology images. Its residual connections promote gradient flow, which aids in the learning of complicated nuclear patterns, which is important in DLBCL analysis. Based on the study by Vrabac et al. [12], they employed ResNet-50 as their chosen pre-trained model.

4) DenseNet-201: DenseNet-201 has a distinct architecture that is advantageous for DLBCL nuclei segmentation. Each layer in DenseNet-201 receives input from all preceding layers, resulting in dense connections throughout the network. This connectivity pattern allows for efficient information flow, which is important for capturing complex nuclear features in DLBCL pathology images. The densely connected blocks of DenseNet-201 allow for feature reuse, increasing model efficiency while effectively separating nuclei. This architecture reduces information loss, which is especially useful when segmenting densely clustered nuclei, which is common in DLBCL samples. According to Basu et al. [13], they used DenseNet-201 as their pre-trained model, optimising it using the Adam optimiser. The learning rate employed was 0.0001 for training.

In the realm of DLBCL nuclei segmentation, various deep learning architectures have been employed to enhance the accuracy and efficiency of pathology image analysis. HoVerNet stands out for its ability to segment clustered nuclei through its multi-branch framework, proving effective in complex arrangements. U-Net, particularly in its 3D form, is widely adopted for its feature extraction and reconstruction capabilities, with several studies optimizing it for large patient datasets. ResNet-50's depth captures intricate nuclear characteristics, while DenseNet-201's dense connectivity ensures comprehensive feature capture and efficient information flow. These architectures, through their unique strengths, contribute significantly to the progress in digital pathology, offering promising avenues for improved diagnostic methods in DLBCL.

While both machine learning and deep learning approaches have shown promise in DLBCL image analysis, they have distinct advantages and limitations. Machine learning techniques, such as MLPs and RBF networks, offer interpretability and ease of implementation but may struggle with capturing complex patterns in high-dimensional data. On the other hand, deep learning approaches, particularly CNNs, excel in learning hierarchical representations directly from raw data but require large amounts of annotated data and computational resources for training.

In short, the choice between machine learning and deep learning approaches in DLBCL image analysis depends on factors such as dataset size, computational resources, and the complexity of the underlying patterns. Integrating both approaches and exploring hybrid models may offer a promising avenue for future research in DLBCL diagnosis and treatment.

IV. DISCUSSIONS

A. Role of Preprocessing and Augmentation

Preprocessing is a cornerstone of successful deep learning applications in DLBCL analysis. Techniques such as Gaussian smoothing, color normalization, and artifact removal ensure consistent image quality across datasets. Hamdi et al. [11] employed Gaussian and Laplacian filters to enhance features, while Graham et al. [19] utilized Otsu thresholding and pixel intensity adjustments to refine segmentation inputs.

Data augmentation further aids in addressing dataset limitations by artificially increasing sample diversity. Techniques such as rotation, flipping, and noise addition have been widely applied. For instance, Wójcik et al. [17] and Swiderska-Chadaj et al. [20] incorporated augmentation strategies to improve model effectiveness and generalizability. However, excessive augmentation risks introducing synthetic artifacts, which could affect real-world applicability.

B. Performance of Deep Learning Models

The performance of HoVerNet and U-Net was evaluated against other deep learning methods, including DenseNet-201 and ResNet-50. HoVerNet and U-Net have emerged as important architectures for nuclei segmentation in DLBCL. HoVerNet's multi-branch framework enables simultaneous segmentation and classification, excelling in cases involving clustered and overlapping nuclei. Studies such as Graham et al. [19] demonstrated its ability to achieve a high Dice score of 0.869 by leveraging nuclear pixel distances and incorporating classification branches. U-Net, on the other hand, employs an encoder-decoder structure that effectively extracts and reconstructs features, as highlighted by Blanc-Durand et al. [14], who used a 3D variant of U-Net for PET/CT imaging.

While these models show promise, their performance heavily depends on preprocessing pipelines. For example, resizing, normalization, and augmentation methods were critical for improving model accuracy in studies like Hamdi et al. [11] and Ferrández et al. [15]. Despite their strengths, challenges such as overfitting, dataset variability, and computational demands remain significant.

C. Challenges and Limitations

Several challenges persist in applying deep learning to DLBCL segmentation such as variability in data quality. The differences in staining protocols and imaging equipment introduce inconsistencies that can affect model performance. Studies like Vrabac et al. [12] underscore the need for standardized preprocessing pipelines. Besides, limited annotated data is one of the limitations. The scarcity of labeled datasets restricts model training and evaluation. Transfer learning and synthetic data generation offer potential solutions but require further refinement. Lastly, computational complexity poses challenges in applying deep learning to DLBCL. Advanced architectures such as HoVerNet demand significant computational resources, which may limit their accessibility in resource-constrained settings.

D. Opportunities and Future Directions

Advancements in artificial intelligence present opportunities to overcome existing challenges. Generative adversarial networks (GANs) can be used to augment datasets with realistic synthetic images, while hybrid models that combine U-net and HoVerNet architectures could leverage the strengths of both. Additionally, transfer learning can facilitate model adaptation across diverse datasets, improving generalizability.

Future research should focus on developing lightweight architectures for resource-limited environments. Besides, establishment of standardized datasets and evaluation metrics for fair benchmarking should carried on. This advancement could significantly enhance the diagnostic accuracy and efficiency of DLBCL analysis, ultimately improving patient outcomes.

V. Conclusion

In conclusion, deep learning approaches have demonstrated their potential as useful and efficient algorithms for segmentation and classification of DLBCL. Based on the literature review, there are some related studies that have been done on the deep learning-based nuclei segmentation of DLBCL. These studies have demonstrated the effectiveness of deep learning in improving DLBCL diagnosis. Thus, it is believed that further exploration and enhancement of the nuclei segmentation and classification will provide a wide alternative way to count and diagnose the severity level of DLBCL. Deep learning offers an alternative to traditional methods, opening opportunities for further research and practical applications.

Institutional Review Board Statement

This study was conducted in accordance with the Declaration of Helsinki and approved by the Jawatankuasa Etika Penyelidikan Manusia Universiti Sains Malaysia (JEPeM-USM), on April 2, 2023. (Approval Reference: USM/JEPeM/22110749).

Acknowledgment

The author thanks the Faculty of Electronic Engineering Technology at Universiti Malaysia Perlis for providing the opportunity to explore deep in this research. The author would like to acknowledge the support from the Ministry of Higher Education (MoHE) Malaysia through the Fundamental Research Grant Scheme (FRGS) under a grant number of FRGS/1/2023/ICT02/UNIMAP/02/3. In most cases, sponsor and financial support acknowledgements. Universiti Sains Malaysia, RU Top Down grant 1001/PPSP/8070016.

References

[1] Diffuse Large B-Cell Lymphoma - Lymphoma Research Foundation. (n.d.). https://lymphoma.org/understanding-lymphoma/aboutlymphoma/nhl/dlbcl/

[2] M. A. Lopez, “Diffuse large B-cell lymphoma risk factors,” Rare Disease Advisor, https://www.rarediseaseadvisor.com/hcp-resource/diffuse-large-b-cell-lymphoma-risk-factors/.

[3] C. C. medical professional, “Diffuse large B-cell lymphoma,” Cleveland Clinic, https://my.clevelandclinic.org/health/diseases/24405-diffuse-large-b-cell-lymphoma.

[4] Larson, D.P., Peterson, J.F., Nowakowski, G.S. et al. (2020). A practical approach to FISH testing for MYC rearrangements and brief review of MYC in aggressive B-cell lymphomas. J Hematopathol 13, 127–135, doi: 10.1007/s12308-020-00404-w.

[5] “Diffuse large B cell lymphoma: Outlook, stages, treatment,” Medical News Today, https://www.medicalnewstoday.com/articles/diffuse-large-b-cell-lymphoma.

[6] Liu, Y., & Barta, S. K. (2019). Diffuse large B-cell lymphoma: 2019 update on diagnosis, risk stratification, and treatment. In American Journal of Hematology (Vol. 94, Issue 5, pp. 604–616). Wiley-Liss Inc, doi: 10.1002/ajh.25460.

[7] M. A. Lopez, “Diffuse large B-cell lymphoma diagnosis,” Rare Disease Advisor, https://www.rarediseaseadvisor.com/disease-info-pages/diffuse-large-b-cell-lymphoma-diagnosis/#:~:text=Laboratory%20Testing%20for%20Diagnosing%20DLBCL&text=The%20comprehensive%20metabolic%20panel%20assesses,elevation%20indicates%20the%20tumor%20burden.

[8] M. Shipra Gandhi, "Diffuse large B-cell lymphoma (DLBCL) workup," Approach Considerations, Flow Cytometry and Genetic Studies, Imaging Studies, https://emedicine.medscape.com/article/202969-workup?form=fpf#c1.

[9] Magaki, S., Hojat, S. A., Wei, B., So, A., & Yong, W. H. (2019). An introduction to the performance of immunohistochemistry. In Methods in Molecular Biology (Vol. 1897, pp. 289–298). Humana Press Inc, doi: 10.1007/978-1-4939-8935-5_25.

[10] Nguyen, L., Papenhausen, P., & Shao, H. (2017). The Role of c-MYC in B-Cell Lymphomas: Diagnostic and molecular aspects. Genes, 8(4), 2–22, doi: 10.3390/genes8040116.

[11] Hamdi, M., Senan, E. M., Jadhav, M. E., Olayah, F., Awaji, B., & Alalayah, K. M. (2023). Hybrid Models Based on Fusion Features of a CNN and Handcrafted Features for Accurate Histopathological Image Analysis for Diagnosing Malignant Lymphomas. Diagnostics, 13(13), doi: 10.3390/diagnostics13132258.

[12] Vrabac, D., Smit, A., Rojansky, R., Natkunam, Y., Advani, R. H., Ng, A. Y., Fernandez-Pol, S., & Rajpurkar, P. (2021). DLBCL-Morph: Morphological features computed using deep learning for an annotated digital DLBCL image set. Scientific Data, 8(1), doi: 10.1038/s41597-021-00915-w.

[13] Basu, S., Agarwal, R., & Srivastava, V. (2022). Deep discriminative learning model with calibrated attention map for the automated diagnosis of diffuse large B-cell lymphoma. Biomedical Signal Processing and Control, 76, 103728, doi: 10.1016/j.bspc.2022.103728.

[14] Blanc-Durand, P., Jégou, S., Kanoun, S., Berriolo-Riedinger, A., Bodet-Milin, C., Kraeber-Bodéré, F., Carlier, T., le Gouill, S., Casasnovas, R. O., Meignan, M., & Itti, E. (2021). Fully automatic segmentation of diffuse large B cell lymphoma lesions on 3D FDG-PET/CT for total metabolic tumour volume prediction using a convolutional neural network. European Journal of Nuclear Medicine and Molecular Imaging, 48(5), 1362–1370, doi: 10.1007/s00259-020-05080-7.

[15] Ferrández, M. C., Golla, S. S. V., Eertink, J. J., de Vries, B. M., Wiegers, S. E., Zwezerijnen, G. J. C., Pieplenbosch, S., Schilder, L., Heymans, M. W., Zijlstra, J. M., & Boellaard, R. (2023). Sensitivity of an AI method for [18F]FDG PET/CT outcome prediction of diffuse large B-cell lymphoma patients to image reconstruction protocols. EJNMMI Research, 13(1), doi: 10.1186/s13550-023-01036-8.

[16] el Hussein, S., Chen, P., Medeiros, L. J., Hazle, J. D., Wu, J., & Khoury, J. D. (2022). Artificial intelligence-assisted mapping of proliferation centers allows the distinction of accelerated phase from large cell transformation in chronic lymphocytic leukemia. Modern Pathology, 35(8), 1121–1125, doi: 10.1038/s41379-022-01015-9.

[17] Wójcik, P., Naji, H., Simon, A., Büttner, R., & Bożek, K. (2023). Learning Nuclei Representations with Masked Image Modelling. http://arxiv.org/abs/2306.17116

[18] Li, D., Bledsoe, J. R., Zeng, Y., Liu, W., Hu, Y., Bi, K., Liang, A., & Li, S. (2020). A deep learning diagnostic platform for diffuse large B-cell lymphoma with high accuracy across multiple hospitals. Nature Communications, 11(1), doi: 10.1038/s41467-020-19817-3.

[19] Graham, S., Vu, Q. D., Raza, S. E. A., Azam, A., Tsang, Y. W., Kwak, J. T., & Rajpoot, N. (2018). HoVer-Net: Simultaneous Segmentation and Classification of Nuclei in Multi-Tissue Histology Images. http://arxiv.org/abs/1812.06499

[20] Swiderska-Chadaj, Z., Hebeda, K. M., van den Brand, M., & Litjens, G. (2021). Artificial intelligence to detect MYC translocation in slides of diffuse large B-cell lymphoma. Virchows Archiv, 479(3), 617–621, doi: 10.1007/s00428-020-02931-4.

[21] Bándi, P., Balkenhol, M., van Ginneken, B., van der Laak, J., & Litjens, G. (2019). Resolution-agnostic tissue segmentation in whole-slide histopathology images with convolutional neural networks. PeerJ, 2019(12), doi: 10.7717/peerj.8242.

[22] "Test Details - Diffuse Large B-Cell Lymphoma (DLBCL) FISH Panel." https://knightdxlabs.ohsu.edu/home/test-details?id=Diffuse+Large+B-Cell+Lymphoma+%28DLBCL%29+FISH+Panel

[23] V. Kasireddy, "Double Hit Lymphomas: Role of Immunohistochemistry in the Era of Florescent in-Situ Hybridization," Blood, Dec. 02, 2016, doi: 10.1182/blood.V128.22.5.405.5405.

[24] Ferrández, Maria C. ; Golla, Sandeep S.V. ; Eertink, Jakoba J. et al. (2023). An artificial intelligence method using FDG PET to predict treatment outcome in diffuse large B cell lymphoma patients. Scientific Reports, 13(1), doi: 10.1038/s41598-023-40218-1

[25] Mohlman, J. S., Leventhal, S. D., Hansen, T., Kohan, J., Pascucci, V., & Salama, M. E. (2020). Improving Augmented Human Intelligence to Distinguish Burkitt Lymphoma from Diffuse Large B-Cell Lymphoma Cases. American Journal of Clinical Pathology, 153(6), 743–759, doi: 10.1093/ajcp/aqaa001.

[26] Farinha, F., & Ioannidis, N. (n.d.). Artifact Removal and FOXP3+ Biomarker Segmentation for Follicular Lymphomas.

[27] Shankar, V., Yang, X., Krishna, V., Tan, B. T., Rojansky, R., Ng, A. Y., Valvert, F., Briercheck, E. L., Weinstock, D. M., Natkunam, Y., Fernandez-Pol, S., & Rajpurkar, P. (n.d.). LymphoML: An interpretable artificial intelligence-1 based method identifies morphologic features that 2 correlate with lymphoma subtype 3 4, doi: 10.1101/2023.03.14.23287143.

[28] Jiang, C., Chen, K., Teng, Y., Ding, C., Zhou, Z., Gao, Y., Wu, J., He, J., Kelei He, &, & Zhang, J. (n.d.). Deep learning-based tumour segmentation and total metabolic tumour volume prediction in the prognosis of diffuse large B-cell lymphoma patients in 3D FDG-PET images, doi: 10.1007/s00330-022-08573-1.

[29] Swiderska-Chadaj, Z., Hebeda, K., van den Brand, M., & Litjens, G. (2020). Predicting MYC translocation in HE specimens of diffuse large B-cell lymphoma through deep learning. 36, doi: 10.1007/s00428-020-02931-4.

[30] Steinbuss, G., Kriegsmann, M., Zgorzelski, C., Brobeil, A., Goeppert, B., Dietrich, S., Mechtersheimer, G., & Kriegsmann, K. (2021). Deep learning for the classification of non-hodgkin lymphoma on histopathological images. Cancers, 13(10), doi: 10.3390/cancers13102419.

[31] Perry, C., Greenberg, O., Haberman, S., Herskovitz, N., Gazy, I., Avinoam, A., Paz-Yaacov, N., Hershkovitz, D., & Avivi, I. (2023). Image-Based Deep Learning Detection of High-Grade B-Cell Lymphomas Directly from Hematoxylin and Eosin Images. Cancers, 15(21), 5205, doi: 10.3390/cancers15215205.

[32] Lisson, C. S., Lisson, C. G., Mezger, M. F., Wolf, D., Schmidt, S. A., Thaiss, W. M., Tausch, E., Beer, A. J., Stilgenbauer, S., Beer, M., & Goetz, M. (2022). Deep Neural Networks and Machine Learning Radiomics Modelling for Prediction of Relapse in Mantle Cell Lymphoma. Cancers, 14(8), doi: 10.3390/cancers14082008.

[33] Carreras, J., Kikuti, Y. Y., Miyaoka, M., Hiraiwa, S., Tomita, S., Ikoma, H., Kondo, Y., Ito, A., Nakamura, N., & Hamoudi, R. (2021). A Combination of Multilayer Perceptron, Radial Basis Function Artificial Neural Networks and Machine Learning Image Segmentation for the Dimension Reduction and the Prognosis Assessment of Diffuse Large B-Cell Lymphoma. AI 2021, Vol. 2, Pages 106-134, 2(1), 106–134, doi: 10.3390/ai2010008.

[34] Carreras, J., Roncador, G., & Hamoudi, R. (2022). Artificial Intelligence Predicted Overall Survival and Classified Mature B-Cell Neoplasms Based on Immuno-Oncology and Immune Checkpoint Panels. Cancers, 14(21), doi: 10.3390/cancers14215318.

[35] Wagner, M., Hänsel, R., Reinke, S., Richter, J., Altenbuchinger, M., Braumann, U. D., Spang, R., Löffler, M., & Klapper, W. (2019). Automated macrophage counting in DLBCL tissue samples: A ROF filter based approach. Biological Procedures Online, 21(1), doi: 10.1186/s12575-019-0098-9.

[36] Chen, P., el Hussein, S., Xing, F., Aminu, M., Kannapiran, A., Hazle, J. D., Medeiros, L. J., Wistuba, I. I., Jaffray, D., Khoury, J. D., & Wu, J. (2022). Chronic Lymphocytic Leukemia Progression Diagnosis with Intrinsic Cellular Patterns via Unsupervised Clustering. Cancers, 14(10), doi: 10.3390/cancers14102398.

[37] Carreras, J., Kikuti, Y. Y., Miyaoka, M., Hiraiwa, S., Tomita, S., Ikoma, H., Kondo, Y., Ito, A., Shiraiwa, S., Hamoudi, R., Ando, K., & Nakamura, N. (2020). A Single Gene Expression Set Derived from Artificial Intelligence Predicted the Prognosis of Several Lymphoma Subtypes; and High Immunohistochemical Expression of TNFAIP8 Associated with Poor Prognosis in Diffuse Large B-Cell Lymphoma. AI (Switzerland), 1(3), 342–360, doi: 10.3390/ai1030023.

[38] Bhattamisra, S. K., Banerjee, P., Gupta, P., Mayuren, J., Patra, S., & Candasamy, M. (2023). Artificial Intelligence in Pharmaceutical and Healthcare Research. In Big Data and Cognitive Computing (Vol. 7, Issue 1). MDPI, doi: 10.3390/bdcc7010010.

[39] Achi, H. el, Belousova, T., Chen, L., Wahed, A., Wang, I., Hu, Z., Kanaan, Z., Rios, A., & Nguyen, A. N. D. (2019). Automated Diagnosis of Lymphoma with Digital Pathology Images Using Deep Learning. www.annclinlabsci.org

[40] "Multi-Layer Perceptron Learning in Tensorflow," GeeksforGeeks, Nov. 03, 2021. https://www.geeksforgeeks.org/multi-layer-perceptron-learning-in-tensorflow/

[41] Kumar Agarwal, A., Angeline Ranjithamani, D., Velayudham, A., Shunmugam, A., & Ismail, M. B. (2021). Machine Learning Technique for the Assembly-Based Image Classification System.

[42] Mohammed Ismail.B, S.Mahaboob Basha, & B.Eswara Reddy. (2015). Improved fractal image compression using range block size. 2015 IEEE International Conference on Computer Graphics, Vision and Information Security (CGVIS) : 2-3 November, 2015, KIIT University, Bhubaneswar, Odisha, India. IEEE.

APPENDIX

TABLE I. SUMMARY OF PRE-PROCESSING AND SEGMENTATION METHODS ON DLBCL

Authors	No of Samples	Pre-Processing Methods	Features Extraction	Data Augmentation	CNN Architecture	Results
Hamdi, M. et al. [11]	15,000 H&E stained whole-slide images.	- Gaussian filter - Laplacian filter - Normalisation - Resize	Yes	Yes	Pre-trained model: - MobileNet-VGG16 - VGG16-AlexNet - MobileNet-AlexNet	MobileNet-VGG16 - AUC: 99.43% - Accuracy: 99.8% - Precision: 99.77% - Sensitivity: 99.7% - Specificity: 99.8%
Vrabac, D. et al. [12]	209 DLBCL cases.	N/A	- Maximum area - Minimum area - Hull area - Perimeter nucleus - Maximum angle - Ellipse perimeter - Ellipse area	N/A	Pre-trained model: - ResNet-50 - HoVerNet	C-index (95% CI) of 0.635 (0.574,0.691)
Basu, S. et al. [13]	1,000 pathologic tissue slides images of DLBCL and non-DLBCL.	N/A	- Attention map feature transformer - Feature fusion	- Image rotation - Horizontal and vertical flip - Zoom scaling - Vertical and horizontal shifts	Pre-trained model: - DenseNet-201 Optimiser: Adam Learning rate: 0.0001	- Accuracy: 98.31 ± 0.5 - Sensitivity: 98.27 ± 0.58 - Specificity: 98.35 ± 0.69
Blanc-Durand, P. et al. [14]	Pre-therapy FDG-PET/CT scans from 733 patients with DLBCL.	- Resampling - Padding - Cropping - Scaling of the PET and CT image data - Adaptive thresholding	- Tumour heterogeneity - Textural features - Total Tumour surfaces - Spatial dispersion	N/A	Pre-trained Model: - 3D U-Net Optimiser: Adam	- Mean DSC: 0.73 ± 0.20 (Median: 0.79) - Jaccard coefficients: 0.68 ± 0.21
Ferrández, M. C. et al. [15]	20 DLBCL patients on a dataset of 296 maximum intensity projection (MIP) images.	- Gaussian filter	- Metabolic tumour volume (MTV) - Standard uptake value (SUV) - Dissemination - Textural features	N/A	Pre-trained Model: - 3D U-Net Optimiser: Adam Epochs: 200 Learning rate: 0.00005 Decay rate: 0.000001	- Training: 0.81 (0.02) - Validation: 0.75 (0.07)

Authors	No of Samples	Pre-Processing Methods	Features Extraction	Data Augmentation	CNN Architecture	Results
el Hussein, S. et al. [16]	10 CLL, 12 aCLL, and 8 RT digitally stained H&E slides from a lymph node excisional biopsy.	N/A	- ROI annotation - Ratio of segmented nuclear contour area to its convex - Hull area	N/A	Pre-trained Model: - HoVerNet	- Accuracy: 0.658 (±0.115)
Wójcik, P. et al. [17]	37,665 H&E stained DLBCL images of size 448×448, divided into 28×28 square patches.	N/A	- Cell Patch Embedding - Patch Aggregation	- Random resize and crop - Colour jittering - Random flip	Pre-trained Model: - HoVerNet Epochs: 800	- F1 Score: 0.939 for Epithelial cells.
Li, D. et al. [18]	Hospital A: 500 DLBCL & 505 non-DLBCL human samples Hospital B: 163 DLBCL & 184 non-DLBCL human samples Hospital C: 204 DLBCL & 198 non-DLBCL human samples	N/A	-Types of lymphomas and hematopoietic tumours - Colour - Morphology - Quality	N/A	- Deep Neural Network Classifiers and pathologists were compared.	- Recall: 100% - Precision: 96% - F1 score: 98%
Graham, S. et al. [19]	24,319 annotated nuclei within 41 colorectal adenocarcinoma image tiles.	N/A	- Nuclear pixel branch - Hover branch - Nuclear classification branch	- Flip - Rotation - Gaussian blur - Median blur	Pre-trained Model: - HoVerNet Optimiser: Adam Epochs: 50 Learning rate: 10^{-4}	- DICE score: 0.869
Swiderska-Chadaj, Z. et al. [20]	H&E-stained slides of 287 DLBCL cases from 11 hospitals.	N/A	N/A	N/A	Pre-trained Model: - U-Net	- AUC: 0.83 (External) - Sensitivity: 0.95 (External) - Specificity: 0.53 (Internal)
Bándi, P. et al. [21]	100 whole-slide images from 10 different tissues.	- Otsu thresholding	- Pixel intensity - Colour - Textural features	- Horizontal mirroring - 90° rotation - Scaling - Colour adjustment - Contrast adjustment - Additive Gaussian noise - Gaussian blur	- FCNN Optimiser: Adam Epochs: 16 Learning rate: 10^{-4} Activation: ReLU	- Dice scores: 0.9775 to 0.9891
Ferrández, M. C. et al. [24]	373 DLBCL patients	- Normalisation - Filtering	N/A	N/A	Pre-trained Model: - 3D U-Net Optimiser: Adam Epochs: 200	- AUC: 0.72 - Sensitivity: 0.59 - Specificity: 0.8

Authors	No of Samples	Pre-Processing Methods	Features Extraction	Data Augmentation	CNN Architecture	Results
					Learning rate: 0.00005 Decay rate: 0.000001 Activation: ReLU	
Mohlman, J. S. et al. [25]	10,818 images from Burkitt Lymphoma (BL) and DLBCL.	- Normalisation - Edge detection	- Notion of deep network pixel level	- Random horizontal flipping of images - Random alteration of contrast	Epochs: 200 Learning rate: 6.5×10^{-5}	Accuracy: 94%
Farinha, F. et al. [26]	2886×2886 high resolution images and patched into 36 patches of equal size (481×481)	N/A	N/A	N/A	Pre-trained Model: - U-Net Optimiser: Adam Epochs: 150 Learning rate: 0.0001 Activation: ReLU	- Linear regression, R2: 0.4688
Shankar, V. et al. [27]	670 lymphoma cases	- Normalisation - Patch-based quality control (PQC) threshold	- Minimum / maximum Feret diameters - Convex hull area - Circulatory - Elongation - Convexity	N/A	Pre-trained Model: - StarDist	Diagnostic accuracy: 64.3%
Jiang, C. et al. [28]	414 DLBCL patients collected from two independent centres in 3D FDG-PET images.	- Threshold - Normalisation	- Convolution number	N/A	Pre-trained Model: - 3D U-Net Epochs: 1000 Learning rate: 0.01 Nesterov momentum: 0.99	- PFS: 64.5% - OS: 73.4%
Swiderska-Chadaj, Z. et al. [29]	91 patients with H&E-stained specimens	N/A	N/A	- Brightness - Contrast - Saturation - Rotation - Gaussian noise - Gaussian blur	Pre-trained Model: - U-Net Optimiser: Adam Epochs: 500 Learning rate: 0.0005	- AUC: 0.77 - Sensitivity: 0.88 - Specificity: 0.66
Steinbuss, G. et al. [30]	84,139 image patches from 629 patients	- Patch-based quality control (PQC) threshold	N/A	N/A	Pre-trained Model: - Efficient-Net	- High accuracy above 95% - Lower BACC with multiple misclassification

Authors	No of Samples	Pre-Processing Methods	Features Extraction	Data Augmentation	CNN Architecture	Results
					Optimiser: Adam Epochs: 50 Learning rate: 10^{-5} *to* 10^{-6}	- Overall BACC up to 95.56%
Perry, C. et al. [31]	32 biopsies from 30 patients	N/A	N/A	- Colour Jittering - Channel shuffle	- Multiple Instance Learning (MIL) Optimiser: Adam Epochs: 20 Learning rate: 0.0001	- AUC: 0.95 - Sensitivity: 87% - Specificity: 100%
Lisson, C. S. et al. [32]	30 patients with histologically proven mantle cell lymphoma who underwent contrast-enhanced CT or PET/CT scans	- Filtering-based feature selection	- 3D volumetric radiomic features	- Random Flip - Gaussian Blur - Gaussian Noise	Pre-trained Model: - 3D SE ResNet - 3D DenseNet Optimiser: Adam Epochs: 100 Learning rate: 0.001	- Overall accuracy of predicting relapse: 64%

TABLE II. SUMMARY OF SEGMENTATION METHODS BY MACHINE LEARNING

Authors	No. of Samples	Features Extraction	Segmentation Techniques	Machine Learning	Machine Learning Library	Results
Carreras, J. et al. [33]	414 cases of DLBCL.	- Mann-Whitney U test - Kaplian-Meier - Multivariate Cox Regression - Hazard ratios / risks	- Trainable Weka Segmentation Method	- Multilayer Perceptron (MLP) - Radial Basis Function (RBF)	- XGBoost	- MLP was more "efficient" than RBF.
Carreras, J. et al. [34]	100 to 293 cases from the lymphoma series of Tokai University Hospital.	- Pearson Chi-Square - Fisher's exact tests - Nonparametric Mann–Whitney U test - Kruskal-Wallis H test - Kaplan–Meier - Log-rank tests - Univariate and multivariate Cox Regression	- Weka Method	- Multilayer Perceptron (MLP) - Radial Basis Function (RBF)	- XGBoost	- Overall accuracy: 100%
Wagner, M. et al. [35]	50 test images for whole tissue samples of DLBCL.	- Grayscale conversion	- Rudin-Osher-Fatemi (ROF) filtering	- Mask R-CNN	N/A	- Manual count: 0.9297
Chen, P. et al. [36]	193 biopsy specimens from 135 patients.	- Solidity feature	- ROI annotation	N/A	- XGBoost	- Accuracy: 0.925 - AUC: 0.978

Authors	No. of Samples	Features Extraction	Segmentation Techniques	Machine Learning	Machine Learning Library	Results
Carreras, J. et al. [37]	100 cases from Western countries diagnosed from nodal DLBCL.	- Gaussian blur - Hessian - Membrane projections - Sobel filter - Difference of Gaussians	N/A	- Multilayer Perceptron (MLP)	N/A	- Successful AI approach in DLBCL
Bhattamisra, S. K. et al. [38]	20,863 genes as the input layer and lymphoma subtypes as the output layer.	N/A	N/A	Multilayer Perceptron (MLP)	N/A	- 58 genes predicted survival with high accuracy. - 10 genes were associated with poor survival and 5 genes with favourable survival.
Achi, H. el et al. [39]	Digital WSIs of H&E-stained slides of 128 cases with a total of 2,560 images	- Data augmentation (Random cropping, image rotation, image inversion) - Max-pooling layers	N/A	N/A	- Support Vector Machine - Neural Network	- Overall accuracy: 95%